Available online at www.sciencedirect.com
ScienceDirect
Journal of the European Ceramic Society 31 (2011) 1541–1548
www.elsevier.com/locate/jeurceramsoc

Synthesis of functional gradient BCP/ZrO_2 bone substitutes using ZrO_2 and BCP nanopowders

Minsung Kim, Rose Ann Franco, Byong-Taek Lee *

Department of Biomedical Engineering and Materials, College of Medicine, Soonchunhyang University, Chungnam 330-930, Republic of Korea

Received 14 January 2011; received in revised form 3 March 2011; accepted 13 March 2011
Available online 7 April 2011

Abstract

BCP/BCP–ZrO_2/ZrO_2 scaffold with a functionally gradient layered structure (FG BCP/ZrO_2) was fabricated by the polymeric sponge replica method and subsequent dipping process. To enhance the compressive strength and bioactive properties of monolithic ZrO_2 scaffold, ZrO_2 and BCP phases were selected as a main frame and surface layer, respectively. The formation of microcracks was significantly decreased by incorporating an intermediate layer consisting of BCP–ZrO_2 phase. The thicknesses of the monolithic ZrO_2, BCP–ZrO_2, and BCP layer were around 10–30 μm, 3–5 μm, and 2–3 μm, respectively. The FG BCP/ZrO_2 scaffold showed highly interconnected pores as well as good material properties, which were 68% porosity and 7.2 MPa of compressive strength. Average pore size of FG BCP/ZrO_2 scaffold was about 220 μm in diameter. From MTT assay and SEM observation of osteoblast-like MG-63 cells, FG BCP/ZrO_2 scaffold showed good cell viability and faster proliferation behavior.

Keywords: Calcium phosphate; Bioceramics; Zirconia; Microstructure; Strength

1. Introduction

Porous scaffolds have been widely used for hard tissue engineering due to their structural resemblance to natural cancellous bone. It is generally agreed that microstructures of highly porous scaffolds with interconnected pores and large surface areas are conducive to the growth of hard tissues because they provide blood for the ingrowth of connective tissue. Especially, the minimum pore size for regeneration of mineralized bone is considered to be greater than 100 μm.[1,2] There are several methods for fabricating scaffold materials, such as polymeric sponge replica,[3] freeze casting,[4] polymer impregnating method,[5] etc. Among them, the sponge replica method is widely used to fabricate desirable microstructures having interconnected pores and large surface areas. As a bone substitute material, calcium phosphate ceramics such as hydroxyapatite (HAp, $Ca_{10}(PO_4)_6(OH)_2$) and tricalcium phosphate (TCP, $Ca_3(PO_4)_2$) have attracted great attention due to their excellent biocompatibility and bioactivity as well as chemical similarity to natural bone. Especially, biphasic calcium phosphate (BCP), which consists of HAp and TCP phase, is considered a more efficient material in the medical field for dental implants, orthopedics, bone fillers, and drug delivery systems due to its controllable biological properties, like the bioresorption rate.[6–9] However, the application area of calcium phosphate ceramics to heavy load-bearing parts has been limited due to insufficient mechanical properties such as strength and fracture toughness.[10,11] Several approaches such as microstructure control or the development of composites by the addition of a secondary phase were developed to enhance the mechanical properties.[12,13] One of the key points that must be considered in these approaches is retaining the superior biocompatibility of calcium phosphate ceramics while employing a second phase.

ZrO_2 has been used as a matrix as well as a reinforcement phase due to its excellent mechanical properties and good biocompatibility.[14–18] However, ZrO_2 has no biological activities such as direct bone bonding properties or osteoconduction behavior.[2] Therefore, surface modification of ZrO_2 using bioactive materials is required. Especially, hydroxyapatite coatings were developed in the 1980s to modify the surfaces of non-bioactive materials. Several techniques have been used for HAp coatings, such as plasma spray coating, sol–gel coating, sputter coating, and the dip coating method.[19–21] When ZrO_2 scaffold is coated with calcium phosphate ceramics, there are several prob-

* Corresponding author. Tel.: +82 41 570 2427; fax: +82 41 577 2415.
E-mail address: lbt@sch.ac.kr (B.-T. Lee).

0955-2219/$ – see front matter © 2011 Elsevier Ltd. All rights reserved.
doi:10.1016/j.jeurceramsoc.2011.03.019

lems such as delamination and microcracks during sintering that occur due to mismatch of their thermal expansion coefficients. In our previous works, a functionally gradient layer structure, i.e., HAp, HAp/(Al_2O_3–ZrO_2), and Al_2O_3–ZrO_2, were developed to overcome those problems.[22]

In this study, a porous monolithic ZrO_2 scaffold, which had a structure similar to that of cancellous bone, was fabricated as a main frame by the polymeric sponge replica method. To enhance its bioactive properties and decrease microcracking, the BCP–ZrO_2 and BCP slurries were coated on the monolithic ZrO_2 scaffold as an intermediate layer and outer layer, respectively. Materials properties, detailed microstructures, and cell growth behavior using MG-63 cells of monolithic ZrO_2 and the functional gradient BCP/BCP–ZrO_2/ZrO_2 (FG BCP/ZrO_2) scaffold were characterized using XRD and FE-SEM techniques.

2. Experimental procedure

2.1. Fabrication of monolithic ZrO_2 scaffold

Monolithic ZrO_2 scaffold was fabricated as a main frame by the sponge replica method. The starting materials included commercial tetragonal ZrO_2 powder (3 mol% Y_2O_3, TZ-3Y, Tosoh, Japan); polyvinyl butyral (PVB, Acros, USA) as a binder; and polyurethane (PU) sponge (60 ppi, HD sponge, Korea). To prepare the ZrO_2 slurry, 5 wt% of PVB was dissolved in ethanol and 10 vol% of ZrO_2 powder was subsequently added while stirring. After homogeneous mixing of the slurry for 1 h, ultrasonic waves were applied to minimize the agglomeration of powder. The polyurethane (PU) sponge was immersed in the prepared slurry to coat the strut with ZrO_2. Then, compressed air was blown onto the sponge to maintain the interconnected pores. The ZrO_2 slurry-coated PU sponge was dried at 60 °C for 1 h, and the dipping and drying steps were repeated three times to achieve complete coating. Then, the ZrO_2 slurry-coated PU sponge was slowly heated to 1000 °C at a heating rate of 1 °C/min and then kept for 2 h in air to remove all organic materials. For densification of the ZrO_2 scaffold, microwave sintering (UMF-01, 2.45 GHz, Unicera, Korea) was carried out at 1500 °C for 10 min at a heating speed of 100 °C/min.

2.2. Multilayer coating

As a starting material, BCP nanopowder was synthesized by the microwave hydrothermal method.[8] To fabricate the multilayer structure, BCP/ZrO_2 (volume fraction 50:50) and BCP slurries were prepared by mixing powder homogeneously in ethanol containing 5 wt% of PVB. The sintered monolithic ZrO_2 scaffold was immersed in the BCP/ZrO_2 slurry and dried at 60 °C for 1 h. This step was repeated twice to obtain the uniform intermediate layer. After heat treatment at 1000 °C for 2 h to remove binder and at 1500 °C for 10 min for sintering, BCP slurry coating was conducted twice to obtain the outer layer. Following the burning out and microwave sintering steps, the multilayer structure was fabricated.

2.3. Characterization and material properties test

X-ray diffraction (XRD, D/MAX-250, Rigaku, Japan) was used to identify the crystal structure and phases of the scaffold. The microstructure and composition of the scaffolds were characterized using a scanning electron microscope (SEM, JEOL, JSM-6701F, Japan) equipped with energy dispersive spectroscopy (EDS). The specimens (7 mm × 7 mm × 4 mm) were subjected to compression tests using a universal testing machine (Unitech^{TM}, R&B, Korea) with a crosshead speed of 0.5 mm/min under ambient conditions. A mercury porosimeter (PoreMaster^{TM}, Quantachrome Instruments, FL, USA) was used to analyze the porosity and pore size distribution.

2.4. In vitro study

To investigate the compatibility of the biomaterial in living systems *in vitro*, MG-63 human osteoblast-like cells were used. Initially, cells were maintained in Dulbecco's Modified Eagle Medium (DMEM: Hyclone, Logan, UT) supplemented with 10% fetal bovine serum and 1% penicillin/streptomycin antibiotics. The adhesion behavior of MG-63 cells was determined by seeding (1×10^6 cells/ml) on the surfaces of the scaffolds. Cell-seeded samples were incubated at 37 °C in 5% CO_2. After 60 min and 5 days of incubation, cell-seeded samples were fixated with 2.0% glutaraldehyde, dehydrated with a graded ethanol series, and then treated with hexamethyldisilazane for critical point drying. Scaffolds were coated with Pt and examined by field emission scanning electron microscopy.

Cytotoxicity of the scaffolds was measured by MTT (3-(4,5-dimethylthiazol-2-yl)-2,5-diphenyltetrazolium bromide) assay using the ISO 10993-5 standard. Cell viability was calculated as the percentage absorbance of treated wells relative to the absorbance of wells without extract solution.

3. Results

3.1. Porous monolithic ZrO_2 scaffolds

Typical microstructures of monolithic ZrO_2 scaffolds using 60 ppi of PU foam are shown in Fig. 1(a–c). The structure of the scaffolds maintained the initial shape of the PU sponge without blocking the pores or collapsing the frame. The pores were spherical in shape, highly interconnected with each other, and distributed throughout the ZrO_2 scaffold. The sizes of the interconnected pores ranged from 120 μm to 600 μm, as shown in Fig. 1(a). The struts of the sintered ZrO_2 scaffolds were approximately 100–250 μm thick. From the cross-sectional image (b), a triangle-shaped hollow space was observed due to the burning out of the PU sponge. After the microwave-sintering step, the ZrO_2 scaffolds were well-densified, and the average grain size was about 300 nm in diameter, as shown in Fig. 1(c). Table 1 shows the results of the morphological analysis of the scaffolds from SEM micrographs and the porosimeter.

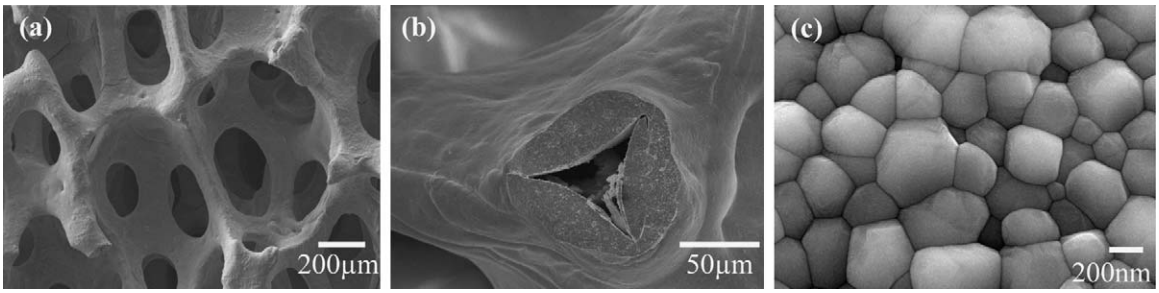

Fig. 1. SEM micrographs of monolithic ZrO_2 scaffold sintered at 1500 °C for 10 min.

Table 1
Morphological characteristics of the scaffolds.

	Pore diameter (μm)	Thickness of strut (μm)	Thickness of outer layer (μm)
ZrO_2	120–600	100–250	10–30
BCP–ZrO_2/ZrO_2	140–600	110–300	3–5
FG BCP/ZrO_2	140–600	110–300	2–3

3.2. Microstructure and sinterability of FG BCP/ZrO_2 scaffold

FG BCP/ZrO_2 scaffolds were fabricated without (a)/with (b and c) the intermediate (BCP–ZrO_2) layer and the effects were observed in Fig. 2. After BCP coating, the spherical pores were well-interconnected with each other without any blocking, as shown in Fig. 2(a and b). The strut of BCP–ZrO_2 scaffold was around 110–300 μm in thickness. When BCP was directly coated onto the monolithic ZrO_2 scaffold, there were many microcracks in the BCP layer (Fig. 2(a)). On the other hand, when the intermediate layer was employed, FG BCP–ZrO_2 scaffold showed remarkably different microstructures, i.e., the BCP layer became very smooth without any microcracks. Furthermore, the surface microstructure of FG BCP/ZrO_2 scaffold was microporous, as shown in Fig. 2(c).

Fig. 3 shows a cross-sectional SEM micrograph of the FG BCP/ZrO_2 scaffold after microwave sintering at 1500 °C for 10 min along with the EDS profiles of each layer. The layers of the FG BCP/ZrO_2 scaffold are clearly marked with arrows and were confirmed to have different morphologies, as shown in Fig. 3(a). The layers were directly bonded to each other without delamination or formation of microcracks between the layers. The thicknesses of the intermediate and BCP layers were around 3–5 μm and 2–3 μm, respectively. Especially, high densification was observed in the intermediate layer. The EDS profiles were obtained from each layer of the strut, as shown in Fig. 3(b–d). The EDS profiles clearly show the relevant elemental peaks of each layer, i.e., Zr and O peaks of the ZrO_2 layer, Zr, O, Ca, and P peaks of BCP–ZrO_2, and Ca, P, and O peaks of BCP were detected.

3.3. Phases and material properties of scaffolds

The XRD profiles of the calcined raw powder at 750 °C (a), along with the monolithic ZrO_2 (b) and FG BCP/ZrO_2 (c) scaffolds sintered at 1500 °C, are presented in Fig. 4. The HAp and β-TCP phases were clearly detected in BCP raw powder (Fig. 4(a)). The phase ratio of BCP powder was calculated by the reference intensity ratio (RIR) method (PDXL, Rigaku, Japan).[23] The RIR values of HAp and β-TCP phases were 68.4 wt% and 31.6 wt%, respectively. Fig. 4(b) shows the XRD profile of sintered monolithic ZrO_2 scaffold; only the ZrO_2 peaks were detected without any other phases. For the FG BCP/ZrO_2 composite, ZrO_2 was detected as a main peak while a little amount of HAp and β-TCP phase was observed. Due to the high sintering temperature, large amounts of HAp and β-TCP phases were transformed to α-TCP phase.

Fig. 5 shows the compressive strength and porosity of the monolithic ZrO_2, BCP–ZrO_2/ZrO_2, and FG BCP/ZrO_2 scaffolds. Monolithic ZrO_2 scaffold without any layer coatings exhibited approximately 86.9% porosity and 4.3 MPa of compressive strength. After the intermediate layer coating, the porosity decreased to around 77%, whereas the compressive strength increased to around 6.6 MPa. By coating the BCP–ZrO_2 layer onto the monolithic ZrO_2 scaffold, an increase in compressive strength of about 50% was achieved only by decreasing the

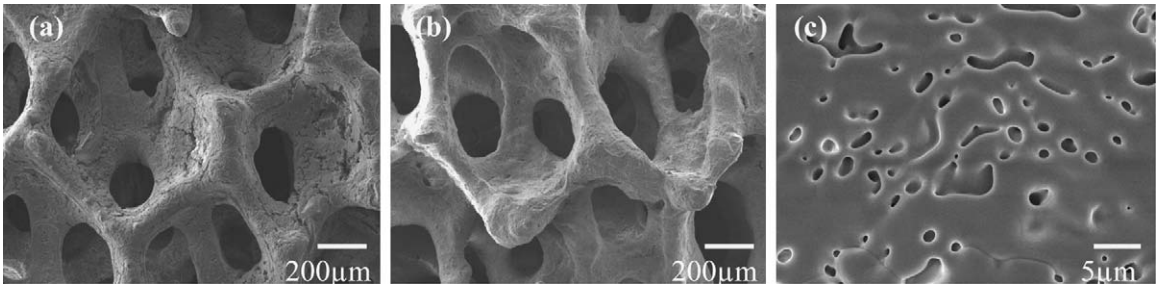

Fig. 2. SEM micrographs of FG BCP–ZrO_2 scaffold without (a)/with (b) intermediate layer.

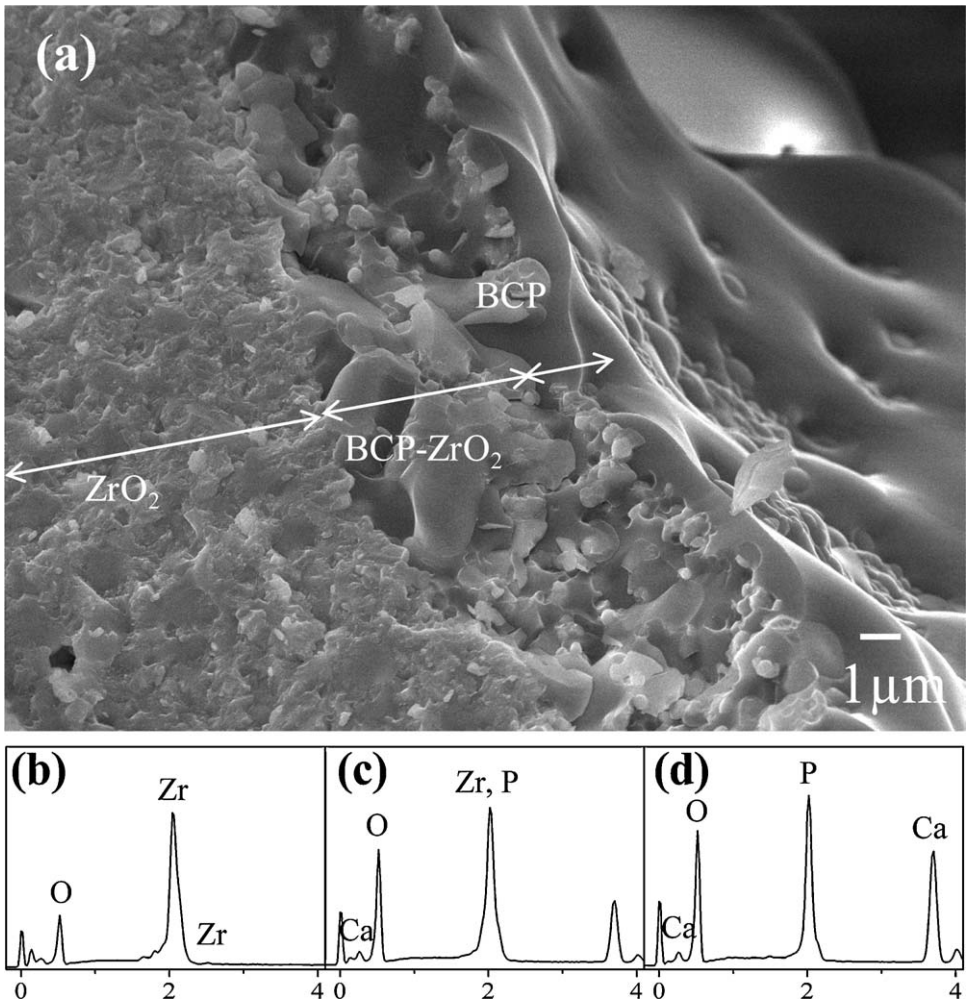

Fig. 3. SEM images and EDS profiles of FG BCP/ZrO_2 scaffolds.

porosity by 9%. However, for the FG BCP/ZrO_2 scaffold, its values were 7.2 MPa and 68.3%, respectively.

The typical pore size distributions are presented in Fig. 6: monolithic ZrO_2 (a) and FG BCP/ZrO_2 (b) scaffolds. The major pore size was from 140 μm to 600 μm in diameter for both the monolithic ZrO_2 and FG BCP/ZrO_2 scaffolds. Especially, pores with diameters between 200 μm and 300 μm were the most prevalent. Furthermore, both scaffolds contained some pores with diameters between 10 μm and 20 μm. These pores were formed due to the removal of the PU sponge. Based on

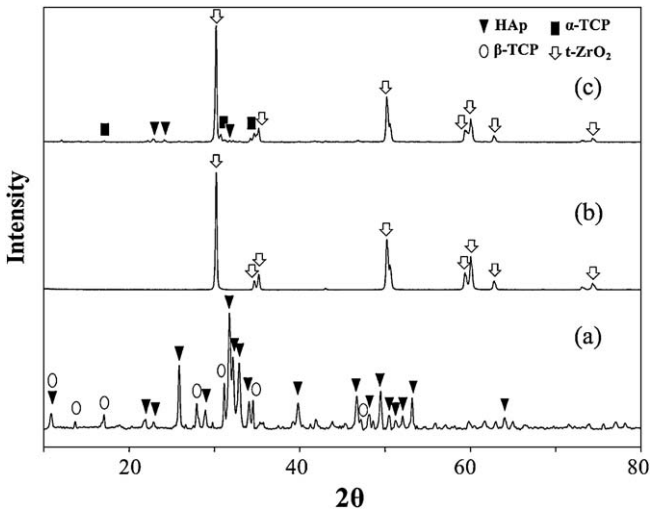

Fig. 4. XRD profiles of BCP raw powder (a), ZrO_2 (b), and FG BCP/ZrO_2 (c) scaffolds.

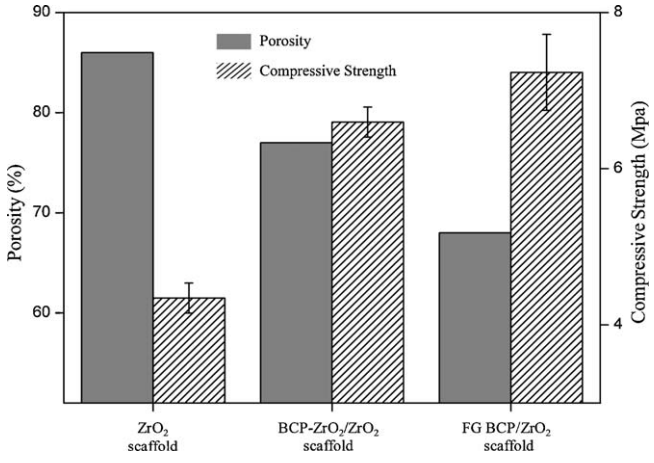

Fig. 5. Material properties of the scaffolds depending on the layer coatings.

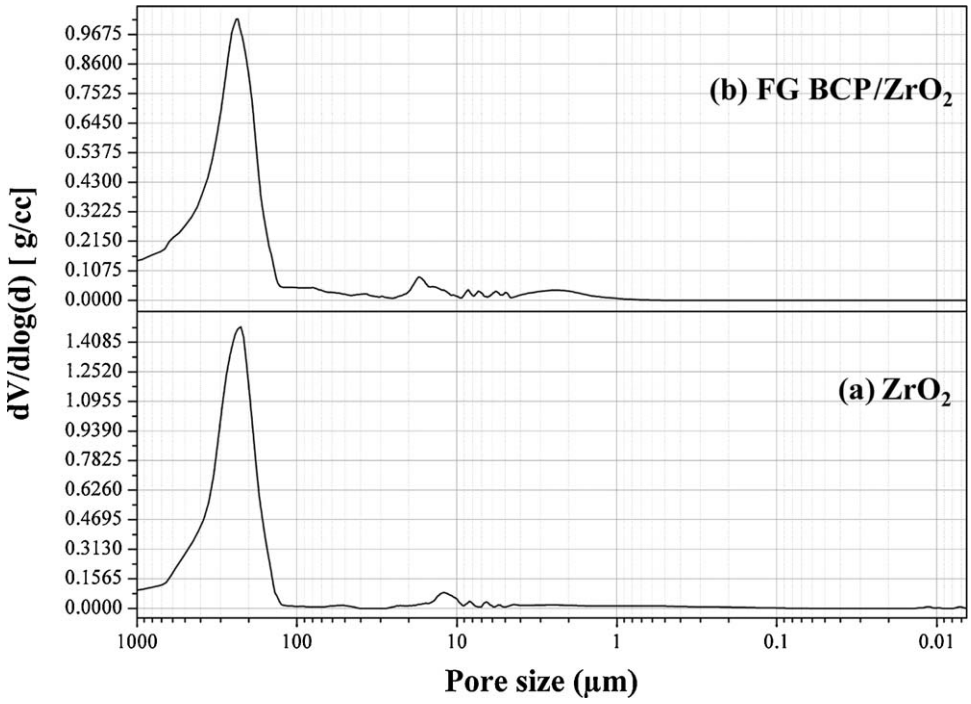

Fig. 6. Pore size distribution of the scaffolds; ZrO_2 (a) and FG BCP/ZrO_2 (b) scaffolds.

our previous research, we confirmed that the scaffolds derived by the sponge replica method always show this range in pore size.

3.4. In vitro study

To assess the preliminary biological properties of the monolithic ZrO_2 and FG BCP/ZrO_2 scaffolds, cell proliferation behavior was observed using MG-63 osteoblast cells. The morphologies of growing cells on the monolithic ZrO_2 (a and c) and FG BCP/ZrO_2 (b and d) scaffolds after 60 min and 5 days of culture are presented in Fig. 7. Extracellular material from osteoblast cells was seen to attach to the scaffold after 60 min of incubation, as evidenced by incremental cytoplasmic projections protruding from the cell center. Significant elongation of the cell body along with cell shape changes were noted as well as attachment of extracellular material to the scaffolds after 5 days of incubation. The manner of extracellular material deposition, however, can be differentiated. The growth of osteoblast cells on the monolithic ZrO_2 scaffold occurred in a bidirectional manner (Fig. 7(c)), whereas centrifugal or outward growth in all directions was observed when monolithic ZrO_2 scaffold was coated with BCP (Fig. 7(d)). Cell growth on the FG BCP/ZrO_2 scaffold was also observed to be denser after 5 days of incubation compared to monolithic ZrO_2 scaffold.

Cytotoxicity of the scaffolds was determined by MTT assay and quantified as the percentage of cell viability against non-treated wells (Fig. 8). It was observed that both scaffolds displayed more than 80% cell viability in all dilutions of the extracted solutions. It was also observed that cell viability increased moderately upon exposure to the extract solution of the FG BCP/ZrO_2 scaffold compared to monolithic ZrO_2.

4. Discussion

In this study, we successfully fabricated a functional gradient porous BCP/ZrO_2 scaffold with excellent mechanical and bioactive properties using ZrO_2 and BCP nanopowders by the sponge replica method. To avoid mismatch of the thermal expansion coefficient and stronger adhesion, the intermediate layer of BCP–ZrO_2 mixture was incorporated.

The obtained scaffolds were characterized by well-interconnected pores, and a high degree of interconnection between the pores allowed subsequent homogeneous multilayer coatings. The average pore diameter in the scaffold was between 200 μm and 300 μm (Fig. 6). It is well known that large pores between 100 μm and 300 μm show significant bone ingrowth.[24] In addition, the BCP layer was found to be porous (Fig. 2(c)), and these pores were found to be between 1 μm and 5 μm by pore size distribution analysis (Fig. 6(b)). Surface roughness and micropores (size <10 μm) play important roles upon implantation of bone substitutes. Micropores contribute to higher protein adsorption during bone formation, and the rough surface enhances cell adhesion, proliferation, and differentiation.[1] Moreover, for a successful implantation of hard tissue, the materials should be bio-active, such that they can be transformed into natural hard tissue. Further, such materials should have optimum porosity and pore size that would allow storage and transmission of bone forming cells throughout the entire scaffold. A high degree of interconnectivity between the individual pores is also very important, as this would make the individual pores available for proliferating cells and physiological fluid. The PU foam was pyrolysed into the final structure along with the coated slurry (Fig. 1(b)). Therefore, the mechanical properties and structural stability of the coating depend on thickness and homogeneity.

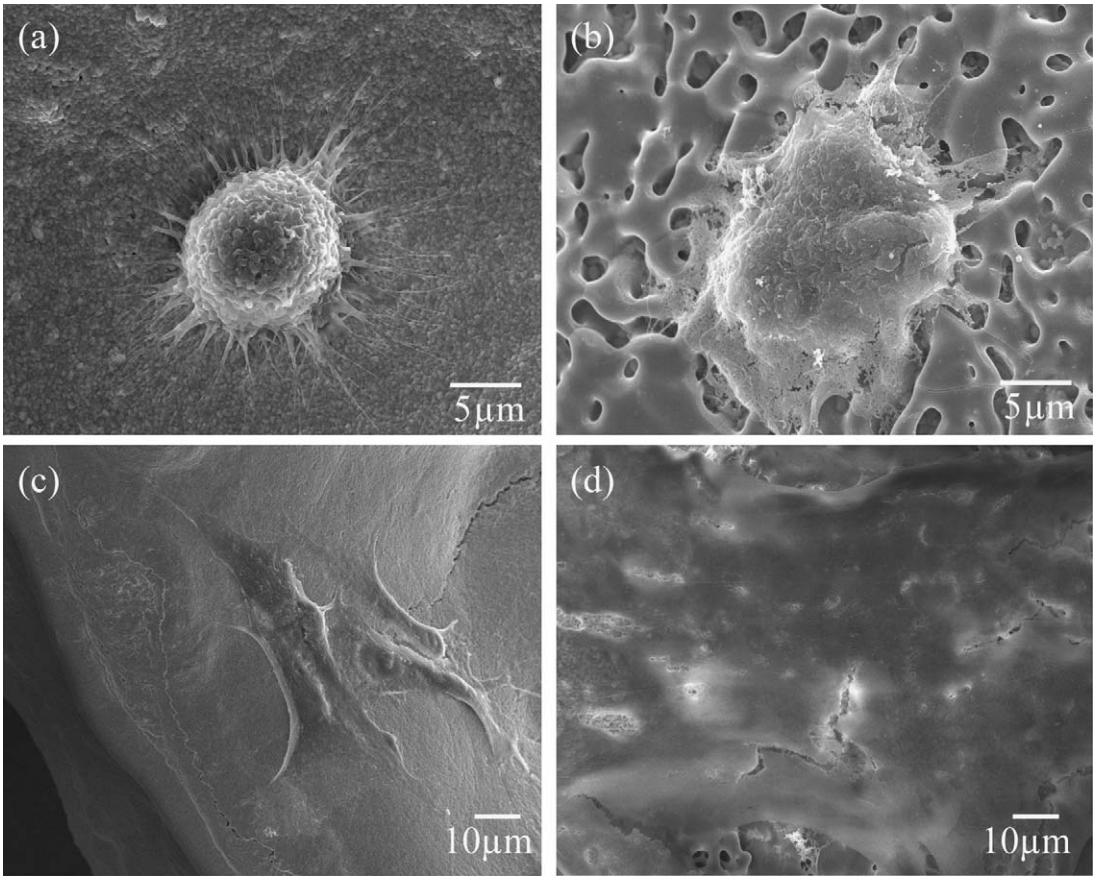

Fig. 7. SEM micrographs of proliferated MG-63 cells on the scaffolds after culturing; (a) ZrO_2 for 60 min, (b) FG BCP–ZrO_2 for 60 min, (c) ZrO_2 for 5 days, and (d) FG BCP–ZrO_2 for 5 days.

The monolithic ZrO_2 scaffold was coated with BCP nanopowder along with a BCP–ZrO_2 layer in order to augment its bioactive properties. One of the main reasons that BCP–ZrO_2 scaffold without the intermediate layer showed poor microstructure was due to mismatch of the thermal expansion coefficient between the BCP and ZrO_2 phases ($\alpha_{HAp} = 13.6 \times 10^{-6}\,^{\circ}C^{-1}$, $\alpha_{t\text{-}ZrO_2} = 10.3 \times 10^{-6}\,^{\circ}C^{-1}$). However, when the intermediate layer was incorporated, the BCP layer showed excellent sinterability without microcracks (Figs. 2 and 3). The intermediate layer can effectively reduce mismatch of the thermal expansion coefficient during the sintering step.[22] The phases of each layers were confirmed by the EDS profiles (Fig. 3(b–d)). The zirconium

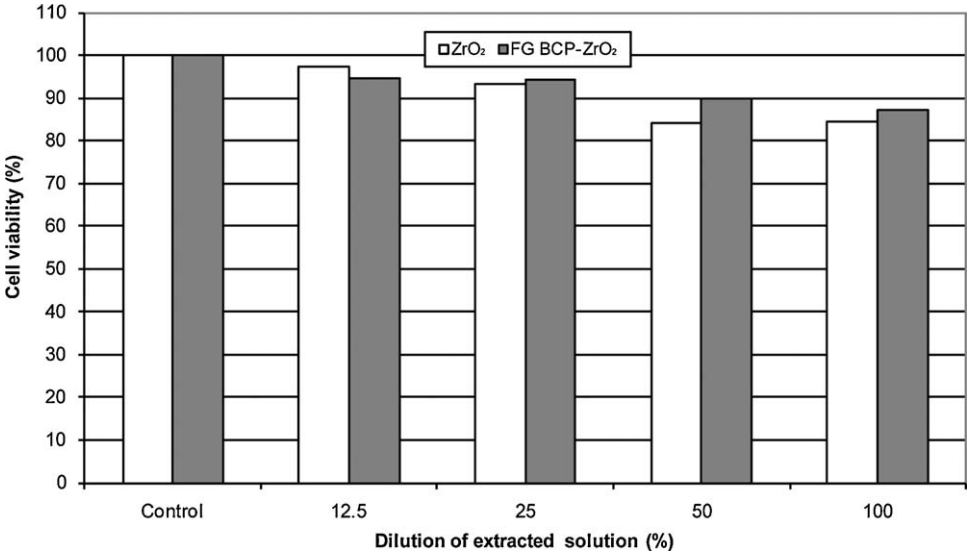

Fig. 8. Cell viability of ZrO_2 and FG BCP/ZrO_2 scaffolds using MTT assay.

peak represents ZrO_2 phase, and calcium peak represent HAp and TCP phases. So, each layer was formed distinctly without any intermixing during the fabrication processes. The thicknesses of the BCP–ZrO_2 and BCP layers were around 3–5 μm and 2–3 μm, respectively, even though they underwent the same number of coatings. Since ZrO_2 and BCP had different shrinkage rates, the layers appeared to have different thicknesses. Moreover, a dense structure for the BCP–ZrO_2 composite layer was achieved using microwave sintering techniques. Typically, it has difficulty of achieve satisfied sinterability of calcium phosphate-zirconia composite, so that several techniques were tried. Furthermore, enhanced sinterability of HAp–ZrO_2 composite was achieved using microwave sintering technique.[25,26] Further, upon BCP layer coating of BCP–ZrO_2/ZrO_2 scaffold, residual pores in the intermediate layer were covered with BCP, which formed a dense microstructure after the final sintering step.

The peak intensity of the ZrO_2 phase was higher due to a high quantity of ZrO_2 and high crystallinity. Most of the HAp and β-TCP phases were transformed to α-TCP phase due to the high sintering temperature of 1500 °C in this process (Fig. 4(c)). Generally, phase transformation of HAp to TCP occurs at temperatures near 1200 °C, while β-TCP phase is also transformed to α-TCP above 1400 °C.[27] α-TCP is considered to be more easily degradable under *in vivo* conditions, and this can lead to fast osteointegration on the scaffold surface.[28]

After multilayer coatings, the scaffolds exhibited improved compressive strength from 4.3 MPa to 7.2 MPa, whereas porosity decreased from 86.9% to 68.3%. Compared to the monolithic ZrO_2 scaffold, this is a significant improvement, as is the improvement in bio-compatibility due to the incorporation of BCP. Dip coatings were repeated two times for each layer, after which it was confirmed that the porosity decreased by approximately 9% after two coatings. Although the porosity decreased, such a material is still acceptable as a scaffold material in clinical applications.[1] On the other hand, when BCP–ZrO_2 layer was coated, the compressive strength increased by around 50%, whereas a little higher value (0.6 MPa increase) was observed upon BCP layer coating. The outer layer imparted little mechanical improvement, but it definitely improved the biological response of the implant in the host site.

It is known that ZrO_2 displays excellent biocompatibility and has been widely used as a bone substitute and dental implant. However, ZrO_2 is a biologically inert material that does not induce a specific host response upon implantation.[24] In this study, BCP was used to coat and improve the bioactivity of monolithic ZrO_2 scaffold. It was observed that the interaction between the implant and host site occurred on the surface of the implant, which is vital to the formation of a biological apatite on which the bone-forming cells perform the regeneration. BCP which consists of a mixture of HAp and TCP is a soluble form of calcium phosphate that has biocompatibility, bioactive, and osteoconductive properties. From the SEM micrographs of cell adhesion and MTT assay (Figs. 7 and 8), it was found out that both samples were able to support cell growth and maintain more than 80% cell viability. However, it is worth noting that cell adhesion and cell viability in the FG BCP/ZrO_2 scaffold improved more than in the monolithic ZrO_2 scaffold. Coating of BCP, therefore, contributes to the improvement of not only the mechanical but also biological properties of monolithic ZrO_2 scaffold as well.

The present approach was used to promote balance between the mechanical properties and biological properties, especially compressive strength and biocompatibility, without compromising the structural integrity of the system, which may occur due to mismatch in the thermal expansion coefficients of the constituent material.

5. Conclusions

Monolithic ZrO_2 scaffold was successfully fabricated by the sponge replica method using 60 ppi of sponge. Multilayer coatings of BCP and BCP–ZrO_2 mixture (volume fraction 50:50 vol%) were employed onto the surface of the porous ZrO_2 scaffold for strengthening and to improve bioactive properties. The sizes of interconnected pores and struts were around 100–250 μm and 110–300 μm after multilayer coatings, respectively. At 1500 °C by microwave sintering, BCP layer showed the highest sinterability, whereas the HAp and β-TCP phases were transformed to α-TCP phase due to high temperature. The intermediate layer effectively decreased the mismatch in thermal expansion coefficient, which consequently helped to prevent any cracks between the layers. The values of porosity and compressive strength were 86.9% and 4.3 MPa in monolithic ZrO_2 scaffold, whereas those in FG BCP/ZrO_2 scaffold were 68.3% and 7.2 MPa, respectively. The *in vitro* experiment showed improved bioactive properties of FG BCP/ZrO_2 scaffold.

Acknowledgements

This work was supported by Mid-career Researcher Program through NRF grant funded by the MEST (2009-0092808) and a grant from the Center for Advanced Materials Processing (CAMP) of the 21st Century Frontier R&D Program funded by the Ministry of Science and Technology (code #: 04K1501-00410), Republic of Korea.

References

1. Karageorgiou V, Kaplan D. Porosity of 3D biomaterial scaffolds and osteogenesis. *Biomaterials* 2005;**26**:5474–91.
2. Hench LL, Bioceramics: from concept to clinic. *Journal of the American Ceramic Society* 1991;**74**(7):1487–510.
3. Jun IK, Koh YH, Song JH, Lee SH, Kim HE. Improved compressive strength of reticulated porous zirconia using carbon coated polymeric sponge as novel template. *Materials Letters* 2006;**60**(20):2507–10.
4. Araki K, Halloran JW. Porous ceramic bodies with interconnected pore channels by a novel freeze casting technique. *Journal of the American Ceramic Society* 2005;**88**(5):1108–14.
5. Eom JH, Kim YW, Song IH, Kim HD. Processing and properties of polysiloxane-derived porous silicon carbide ceramics using hollow microspheres as templates. *Journal of the European Ceramic Society* 2008;**28**(5):1029–35.
6. Suchanek W, Yoshimura M. Processing and properties of hydroxyapatite-based biomaterials for use as hard tissue replacement implants. *Journal of Materials Research* 1998;**13**(1):94–117.

7. Varma HK, Sivakumar R. Dense hydroxy apatite ceramics through gel casting technique. *Materials Letters* 1996;**29**(1–3):57–61.
8. Lee BT, Youn MH, Paul RK, Lee KH, Song HY. In situ synthesis of spherical BCP nanopowders by microwave assisted process. *Materials Chemistry and Physics* 2007;**104**:249–53.
9. Kwon SH, Jun YK, Hong SH, Kim HE. Synthesis and dissolution behavior of [beta]-TCP and HA/[beta]-TCP composite powders. *Journal of the European Ceramic Society* 2003;**23**(7):1039–45.
10. de Groot K. Mechanical failure of artificial teeth made of dense calcium hydroxylapatite. In: *Paper presented*. 1981.
11. Suchanek W, Yashima M, Kakihana M, Yoshimura M. Hydroxyapatite ceramics with selected sintering additives. *Biomaterials* 1997;**18**(13):923–33.
12. Yoshida K, Hashimoto K, Toda Y, Udagawa S, Kanazawa T. Fabrication of structure-controlled hydroxyapatite/zirconia composite. *Journal of the European Ceramic Society* 2006;**26**(4–5):515–8.
13. Heisel C, Silva M, Schmalzried T. Bearing surface options for total hip replacement in young patients. *The Journal of Bone and Joint Surgery* 2003;**85**(7):1366.
14. Lee BT, Kang IC, Cho SH, Song HY. Fabrication of a continuously oriented porous Al_2O_3 body and its in vitro study. *Journal of the American Ceramic Society* 2005;**88**(8):2262–6.
15. Huang SG, Vleugels J, Li L, Van der Biest O, Wang PL. Composition design and mechanical properties of mixed (Ce,Y)-TZP ceramics obtained from coated starting powders. *Journal of the European Ceramic Society* 2005;**25**(13):3109–15.
16. Christel P, Meunier A, Heller M, Torre JP, Peille CN. Mechanical properties and short-term in vivo evaluation of yttrium-oxide-partially-stabilized zirconia. *Journal of Biomedial Materials Research Part A* 1989;**23**(1):45–61.
17. Garvie RC, Hannink RH, Pascoe RT. Ceramic steel? *Nature* 1975;**258**(5537):703–4.
18. Chevalier J. What future for zirconia as a biomaterial? *Biomaterials* 2006;**27**(4):535–43.
19. Sun L, Berndt CC, Gross KA, Kucuk A. Material fundamentals and clinical performance of plasma-sprayed hydroxyapatite coatings: a review. *Journal of Biomedical Materials Research* 2001;**58**(5):570–92.
20. Miao X, Hu Y, Liu J, Huang X. Hydroxyapatite coating on porous zirconia. *Materials Science and Engineering: C* 2007;**27**(2):257–61.
21. Ioku K, Yoshimura M, Somiya S. Microstructure and mechanical properties of hydroxyapatite ceramics with zirconia dispersion prepared by post-sintering. *Biomaterials* 1990;**11**(1):57–61.
22. Lee BT, Kim KH, Youn HC, Song HY. Functionally gradient and microchanneled Al_2O_3–(t-ZrO_2)/HAp composites. *Journal of the American Ceramic Society* 2007;**90**(2):629–31.
23. Bish DL, Howard SA. Quantitative phase analysis using the Rietveld method. *Journal of Applied Crystallography* 1988;**21**: 86–91.
24. Hulbert SF, Young FA, Mathews RS, Klawitter JJ, Talbert CD, Stelling FH. Potential of ceramic materials as permanently implantable skeletal prostheses. *Journal of Biomedical Materials Research* 1970;**4**(3): 433–56.
25. Fang Y, Roy DM, Cheng J, Roy R, Agrawal DK. Microwave sintering of hydroxyapatite-based composites. In: Clark DE, Tinga WR, Laia FR, editors. *Ceramic transactions 36*. Westerville, OH: American Ceramic Society; 1993. p. 397–407.
26. Ioku K, Yoshimura M, Sōmiy S. Microstructure and mechanical properties of hydroxyapatite ceramics with zirconia dispersion prepared by post-sintering. *Biomaterials* 1990;**11**(1):57–61.
27. Carrodeguas RG, De Aza AH, Turrillas X, Pena P, De Aza S. New approach to the beta → alpha polymorphic transformation in magnesium-substituted tricalcium phosphate and its practical implications. *Journal of the American Ceramic Society* 2008;**91**(4):1281–6.
28. Dorozhkin SV, Epple M. Biological and medical significance of calcium phosphates. *Angewandte Chemie International Edition* 2002;**41**(17):3130–46.